Scattering Metal Waveguide Based Speckle-Enhanced Prism Spectrometry

Sakir Kaan Çetindağ, Muhammed Fatih Toy, Onur Ferhanoğlu, and Fehmi Çivitci

***Abstract*—We present an optical efficiency improved speckle spectrometer where a scattering metal wave-guide is utilized along with a conventional prism spectrometer. We conducted extensive tests on 25 different scatterers, involving a variety of nanoparticle concentrations, scattering layer thicknesses, and wave-guide vs. non-guiding type scatterers. We observed 35 pm spectral resolution at 1.3% optical efficiency, which we could only achieve with ∼0.01% optical efficiency using a conventional non-guiding scatterer. Thus our new implementation provides up to two orders of magnitude improvement in optical efficiency at the same spectral resolution, as opposed to scatterers that are not sandwiched between metal plates. The improvement in optical efficiency allows for rapid (∼5 μsec exposure) acquisition of the spectrum with a conventional CMOS camera. Thanks to its excellent spectral resolution and diminished optical losses, the proposed spectrometer could be utilized in high frame-rate, real time spectrum reconstruction applications, such as Optical Coherence Tomography.**

***Index Terms*—Optical waveguides, optoelectronic and photonic sensors, spectroscopy.**

I. Introduction

SPECKLE Spectrometry relies on mapping a wavelength-dependent speckle pattern on an image sensor, offering unprecedented spectral resolution [1], [2]. In an effort to improve the spectral range, while preserving the superior spectral resolution that speckle spectrometers possess, we previously demonstrated a speckle-enhanced prism spectrometer (SEPS), showcasing simultaneous use of a prism spectrometer and a scattering medium [3]. Thanks to the prism, the wavelength-dependent spectral patterns are mapped to different spatial locations ensuring high speckle contrast, as opposed to a typical speckle spectrometer that maps the entire spectrum to the same area on the sensor array. With the proposed SEPS, we've demonstrated up to x100 improvement in spectral resolution as opposed to a conventional prism spectrometer, and theoretically unlimited spectral range (practically limited by the size and the wavelength sensitivity of a sensor array). Yet both spectral range and resolution benefits are earned at the expense of optical efficiency that is diminished due to light extinction at the scattering (and also possibly weakly absorbing) medium. The light loss necessitates higher exposure durations at the sensor array, hampering the ability to perform real-time acquisition of the spectrum.

In this study, we incorporate the scattering medium, sandwiched between two planar reflecting surfaces to mitigate potential losses, offering faster data acquisition, paving the way for the adaptation of SEPS in a greater number of applications.

II. Experimental Setup

Fig. 1 illustrates the SEPS setup, showing both conventional (non-guiding) and waveguide scatterers. The setup consists of two cylindrical lenses (having foci of 70-mm and 80-mm, respectively) placed after the light source (Sacher Lasertechnik/TEC-500-0850-030-M), where the light hits the scatterer at the focus. The conventional scatterer basically consists of a titanium dioxide (TiO_2) nanoparticle – epoxy mix sandwiched in between two glass slides. On the other hand the waveguide scatterer is formed by sandwiching the mix in between two, 5 mm × 5 mm gold on silicon dies. The non-guiding scatterer is placed such that optical axis is obliquely incident on the glass slides whereas the metal plates of the waveguide scatterer are parallel to the optical axis to enable coupling of light. Finally, the light is collimated after exiting the scatterer, and focused once again onto the CMOS camera with the third cylindrical lens (having 100-mm focus).

A variety of scatterers (N = 25) are built through mixing nanoparticles (NP) and epoxy at different ratios, and placing cylindrical spacers with different radii, in between the glass or metal (gold evaporated on silicon) plates. Table I provides information regarding the properties of all 25 scatterers.

We conducted experiments to test i) spectral resolution and ii) optical efficiency. Optical efficiency is simply deduced based on the ratio of optical power exiting the waveguide to the optical power impinging upon the waveguide. Note that the measured optical efficiency is also a good indicator of the efficiency of the total system, as other optical components show negligible losses when coated with proper anti-reflection coatings.

Manuscript received June 24, 2019; revised October 14, 2019 and November 27, 2019; accepted December 2, 2019. Date of publication December 11, 2019; date of current version April 1, 2020. This work was supported by the Scientific and Technological Research Council of Turkey TUBITAK under Grant 116F142. *(Corresponding author: Onur Ferhanoğlu.)*

S. K. Çetindağ is with the Department of Electronics and Communication Engineering, Istanbul Technical University, Istanbul 34469, Turkey, and also with IMEC, 3001 Leuven, Belgium (e-mail: cetindag.kaan@gmail.com).

M. F. Toy is with the Department of Biomedical Engineering, Istanbul Medipol University, Istanbul 34810, Turkey (e-mail: mftoy@medipol.edu.tr).

O. Ferhanoğlu is with the Department of Electronics and Communication Engineering, Istanbul Technical University, Istanbul 34469, Turkey (e-mail: ferhanoglu@itu.edu.tr).

F. Çivitci is with Knight Cancer Institute, Oregon Health and Science University, Portland, OR 97239 USA, and also with the Department of Electronics and Communication Engineering, Istanbul Technical University, Istanbul 34469, Turkey (e-mail: fehmi.civitci@gmail.com).

Color versions of one or more of the figures in this article are available online at http://ieeexplore.ieee.org.

Digital Object Identifier 10.1109/JLT.2019.2959140

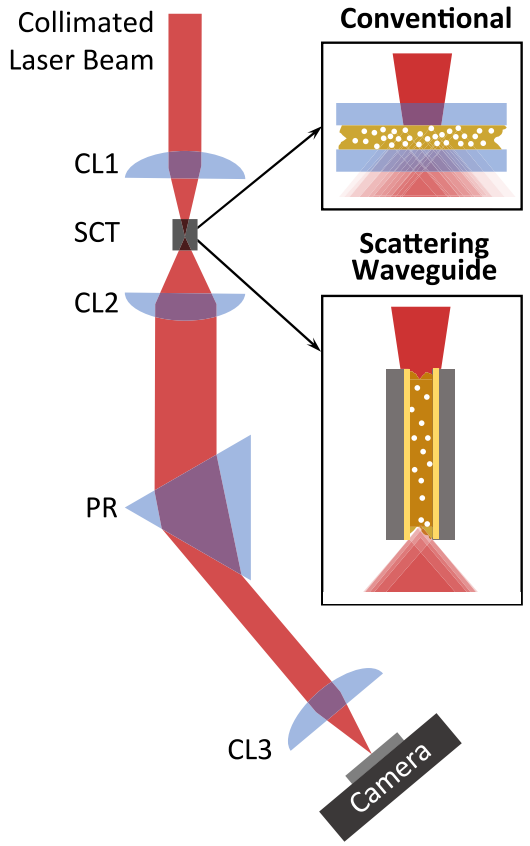

Fig. 1. Optical architecture of the speckle-enhanced prism spectrometer with a conventional scatterer or scattering waveguide (SCT). Setup comprises a light source, three cylindrical lenses (CL1-3), a prism (PR), and a CCD camera (CAM).

TABLE I
SCATTERERS EXPERIMENTED

Type	Scatterer number	Length (μm) *	epoxy/NP mass ratio
Conventional	1-5	125	5, 12, 25, 50, 75
Conventional	6-10	250	5, 12, 25, 50, 75
Conventional	11-15	400	5, 12, 25, 50, 75
Conventional	16-20	750	5, 12, 25, 50, 75
Waveguide	21-25	5000	1000, 2000, 10000, 20000, 50000

*Distance that the light travels. Taken as the thickness for the conventional scatterers and length of the waveguide for waveguide scatterers.

III. Spectral Correlation and Reconstruction

The spectral resolution for each scatterer was calculated based on the half-width half maximum (HWHM) of the spectral correlation function: C(Δλ, x) [4];

$$C(\Delta\lambda, x) = \frac{\langle I(\lambda, x)\, I(\lambda + \Delta\lambda, x)\rangle}{\langle I(\lambda, x)\, I(\lambda + \Delta\lambda, x)\rangle} - 1 \qquad (1)$$

where I(λ, x) denotes the recorded intensity for a given wavelength (λ) and position (x), Δλ refers to the wavelength difference among different recorded speckle patterns for which the correlation is calculated. Note that ⟨.⟩ is the mean operation and

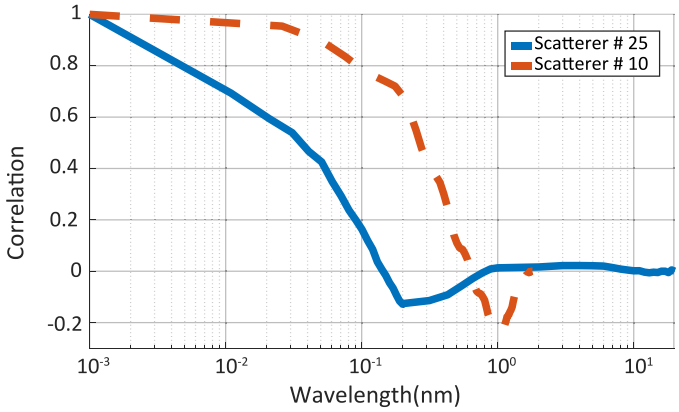

Fig. 2. Spectral correlation functions for a chosen waveguide scatterer (# 25) and non-guiding conventional scatterer (#10).

that the spectral correlation function is calculated through setting Δλ to be the wavelength difference that corresponds to a shift of full-width half-maximum width of the focused speckle line that is observed on the camera, i.e., the spectral resolution of the prism spectrometer itself [3].

The speckle pattern due to a broad-band light source can be expressed as a weighted sum of the speckle patterns acquired for a number of wavelengths with a narrowband tunable source as;

$$I(x) = \int S(\lambda)\, T(\lambda)\, d\lambda \qquad (2)$$

$$I = T \,.\, S \qquad (3)$$

where I(x) is the intensity of the captured image for the broad-band source as a function of position, T(λ) is the transmission for each wavelength, i.e., the speckle patterns acquired for different wavelengths, and S(λ) corresponds to the weights for each wavelength, which is the spectrum that is being reconstructed. Equation (3) represents the matrix form of Eq. (2). Finally, the spectrum can be found with an inverse operation:

$$S = T^{-1}.\, I \qquad (4)$$

Note that the matrix inverse operation requires singular value decomposition (SVD), and truncation of the values of the diagonal matrix resultant of the SVD, to ensure error-mitigated reconstruction.

In this study, we will rather focus on measuring the spectral resolution and the optical transmission to showcase the benefits of using a scattering waveguide. The algorithm behind the reconstruction for waveguide scatterers is no different then conventional scatterers, thus we refer the reader to other publications [3], [4].

IV. Results

We first compare the spectral resolution for two selected samples, first one being a non-guiding scatterer (scatterer #10) whereas the other one being a wave-guide scatterer (scatterer #25). The compared two scatterers result in nearly identical

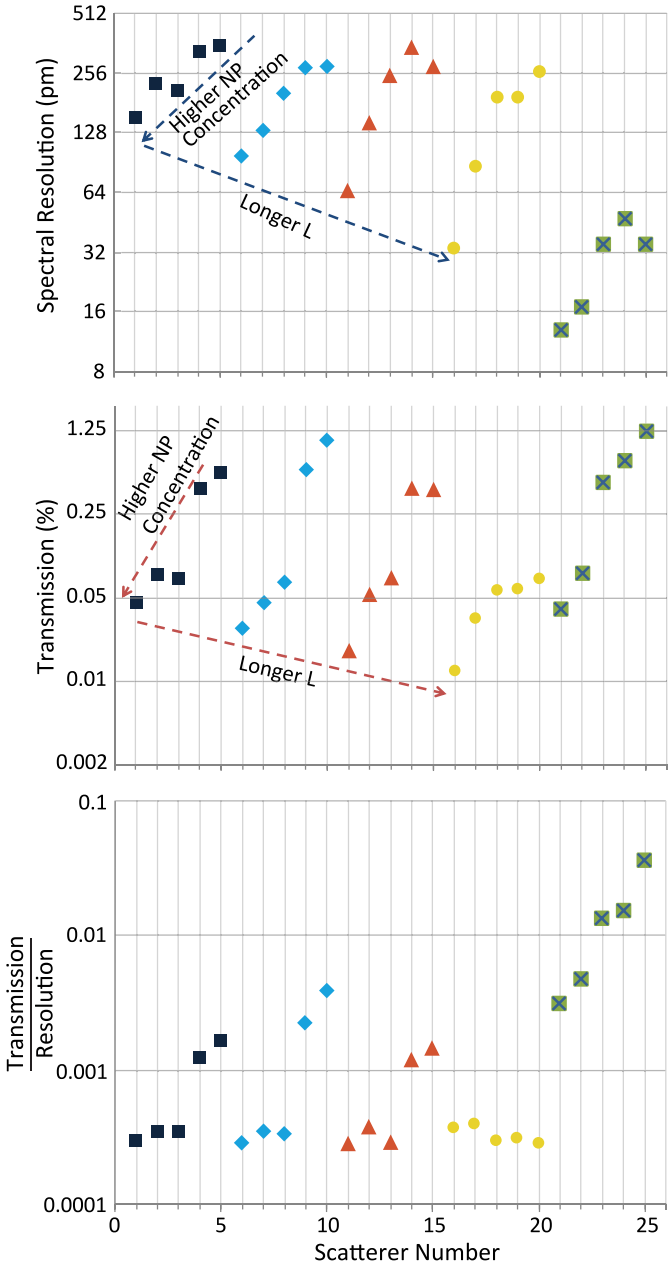

Fig. 3. Comparison of all non-guiding and waveguide scatterers (shaded areas in all graphs) in terms of (a) spectral resolution and (b) optical efficiency, where L is the scatterer length (c) optical efficiency to spectral resolution ratio. In the graphs, each symbol (square, diamond, triangle, circular, crossed square) represents the class of scatterers having the same length.

optical efficiency of ∼1.3%. Fig. 2 illustrates spectral correlation plot for both scatterers.

The correlation graphs indicate nearly 8 fold improvement of the spectral resolution from 276 pm to 35 pm. On the other hand, for two other scatterers having near identical spectral resolution of 35 pm, the waveguide scatterer (#25) shows two orders of magnitude higher optical efficiency, as opposed to the non-guiding scatterer (#16), as later showcased in Fig. 3.

Fig. 3 compares all 25 scatterers based on their spectral resolution, transmission, and transmission to spectral resolution ratio as an overall merit parameter to compare the scatterers. For all conventional scatterers, the length of the scattering medium improves the spectral resolution and diminishes the optical efficiency (for fixed NP concentration), as expected. Furthermore, an increase in the NP concentration results in an improvement (decrease) of the spectral resolution, at the cost of a decrease in the optical transmission. Transmission to spectral resolution ratio is nearly constant for the majority of conventional scatterers. Low NP concentration non-guiding scatterers possess higher transmission to spectral resolution ratio, meaning that the improvement in the optical efficiency dominates the degradation of the spectral resolution in dilute scatterers.

As for the waveguide scatterers, extremely diluted samples still result in a spectral resolution that is equivalent to the most concentrated conventional scatterer. We observe the best spectral resolution as ∼15–50 pm for the waveguide scatterers despite having much lower NP concentration than the non-guiding scatterers. Overall, we observe that a waveguide scatterer showcases a significantly improved optical efficiency to spectral resolution ratio, as observed in Fig. 3(c).

V. Acquisition Time and Light Budget Optimization

In this section, we investigate potential factors to enable data acquisition at lower light levels which will in turn enable faster acquisition time: i) the effect of the height of the field-of-view (FOV), i.e., the selected area (whose relation to desired light intensity will be explained later), and ii) the effect of light intensity in spectral resolution calculations. The experimental results were reported based on a FOV having 1000 pixel height (nearly the entire vertical size of the camera) and a maximum light intensity (of the bright speckles) of 2^{14} levels, addressing the full well depth of our camera pixels.

Fig. 4(a) illustrates the captured speckle pattern for scatterer # 25, while Fig. 4(b), show the change of the spectral resolution as a function of vertical size of the selected FOV and camera bit depth. We observe that the smallest spectral resolution of 35 pm achieved at the maximum FOV height of 1000 pixels, while a spectral resolution of <40 pm could still be attained with a FOV having an x8 diminished height (125 pixels). Thus, a simple variation in the optical components will enable directing 1/8 of the utilized light power, to a limited portion of the FOV (1/8 of the FOV height).

Moreover, through simulations we show in Fig. 4(b) that using a much lower light intensity that fills only 8 bits (256 intensity levels) as opposed to 14 bits (16384 intensity levels) of well depth as done in the experiments to represent speckle pattern (assuming a 3-bit dark-noise limited data as observed in the experiments) is adequate to achieve nearly identical spectral resolution. At lower intensity levels the wavelength dependent noise correlation dominates, resulting in a seemingly lower spectral correlation, which does not anymore reflect the resolution of the spectrometer.

Overall, it is x512 advantageous in terms of the utilized exposure time, through lowering the light intensity by 64 folds (using 8 bit intensity levels as opposed to 14 bits), and 1/8 of the total number of rows in the captured image (implying a 8 fold reduction in the light power). In the upcoming paragraphs,

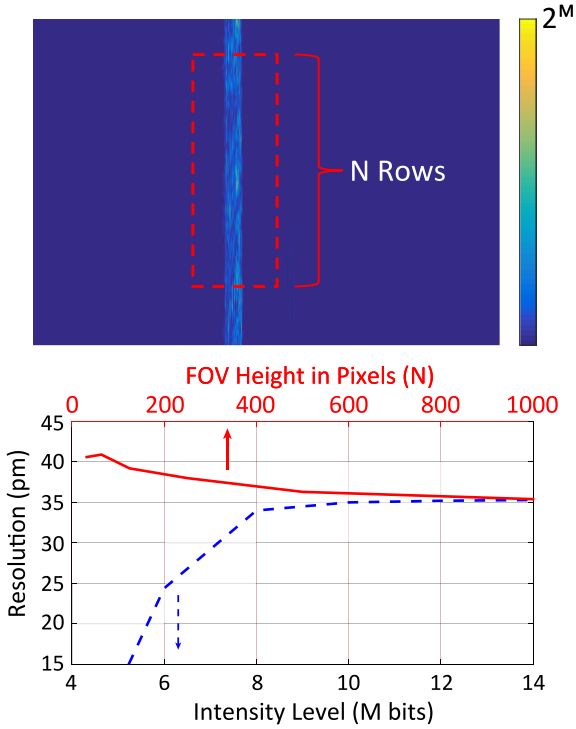

Fig. 4. (a) The speckle pattern and rectangular FOV utilized in calculation of the speckle correlation, on the CCD camera for scatterer # 25 (b) spectral resolution as a function of FOV height (in pixsels) and utilized light intensity (for the camera having 14-bit well depth).

we will rather treat the advantages in using a smaller FOV and smaller bit depth in light budget perspective.

VI. Light Budget Calculations

The essential purpose in introducing a scattering waveguide in the SEPS was to enhance optical efficiency while retaining resolution and dynamic range. In this section, we discuss the possibility and hurdles of utilizing scattering waveguide SEPS in a selected application; ophthalmologic OCT imaging that is particularly challenging due to the restriction of light power impinging the eye due to safety concerns. Without loss of generality the light budget calculations introduced in this section can be performed for other applications that utilize spectrometers. Yet, with its wide clinical adaptation and immense OCT-related scientific publications that has been ongoing in the last three decades, OCT sets a great example to showcase benefits of the proposed metal-waveguide based SEPS.

Fig. 5 illustrates a conceptual spectral OCT system, which is a combination of an interferometer, and scattering waveguide SEPS.

Coherence length or imaging depth (Δz) in a white light interferometer such as an OCT system, is inversely proportional to the wavelength step that could be detected corresponding to the spectral resolution [5]:

$$\Delta z = \frac{\lambda^2}{4n\delta\lambda} \tag{5}$$

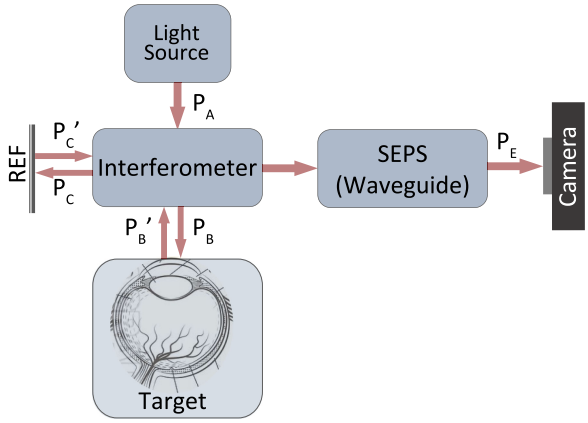

Fig. 5. An OCT system incorporating SEPS as a spectrometer.

where $\lambda = 855$ nm is the center wavelength, n is the refractive index of the medium, typically taken as 1.33 for near Infrared (NIR) band [6]. For scatterer # 25, showcasing the best transmission/resolution performance among all other scatterers, having a spectral resolution of $\delta\lambda = 35$ pm, the imaging depth (Δz) is calculated to be 3.88 mm. Note that scattering and absorption properties of the tissue significantly hampers the imaging depth depicted in Eq. 5, typically to 300–500 μm [7]. Yet, recent advances in adaptive optics and wavefront shaping fields has allowed for significant improvement in the depth that light can penetrate [8].

Our experiments for scatterer # 25, depicted in Figs. 2 and 3, were conducted under $\sim$10 μW power at the camera at 5 μsec exposure time, implying a depth scan rate (A-scan) of 200 kHz. Although the CCD camera we employed is far from matching such a high frame-rate, off-the-shelf high-frame-rate 1.5D line sensors (sensors having much higher number of columns than rows, i.e., 2000 $\times$ 192 pixels) are already available, having similar pixel sizes to the CCD camera we employed. Having already shared the seemingly independent results on the effect of reduced number of rows (up to a certain extent) within the FOV on the spectral resolution, line cameras will be a perfect fit for our the OCT application.

In our optical power budget model, we assume a light source power of $P_A = 1$ mW (matching the experimental conditions). The interferometer unequally divides the beam, ensuring a maximum power of: $P_B = 780$ μW impinges upon the eye, in accordance with safety precautions [9]. We assume that the light travels at a depth (d) that is equal to three scattering lengths ($d = 3l_s$) back and forth (considering the fact that scattering is dominant over absorption in the eye [10] within the tissue, in accordance with the Beer-Lambert Law [11]:

$$P'_B = P_B e^{-2d/l_s} \tag{6}$$

where $P_B{}'$ is the back-scattered light from the eye. The reflected light power from the reference arm of the interferometer taken as $P_C{}' \approx P_B{}' \approx P_D/2$. Finally the total power observed by the camera (P_E) is linked to the power entering the proposed spectrometer (P_D) also by the Beer-Lambert law. The light power exiting the scattering waveguide is 1.23% (the optical efficiency

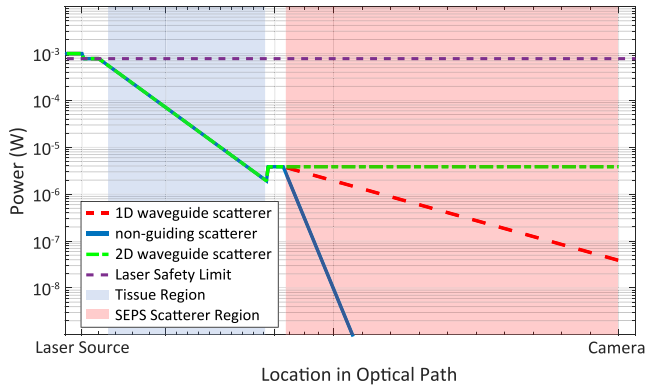

Fig. 6. An example power budget calculation for the scattering waveguide (scatterer #25), non-guiding scatterer (scatterer #10), and the ideal power budget for 2D scattering waveguide.

of the waveguide) of the input power to the waveguide, for scatterer # 25. In light of these arguments the optical power levels from light source to camera are plotted in Fig. 6. The shaded areas in Fig. 6 refer to exponential decrease of the light power in accordance with Beer-Lambert Law due to the turbid tissue and scattering layer. Three scenarios for the scattering layer are compared, namely a non-guiding scatterer, 1D waveguide scatterer (this work), and an ideal 2D wave-guide scatterer (as a future work to implement).

In our experiment, which did not involve any turbid tissues, 10 μW power at the camera could be captured with 5 μsec exposure time. As also discussed in the previous section, mapping the light to 1/8 of the number of vertical pixels (that could be ideally done while reducing the light power to 1/8 of its original value), and another 1/64 deduction of light power (mapping 8 bit intensity levels as opposed to 14 bits), a total of 512 folds less light power of $\sim$20 nW at the camera (as opposed to 10 μW) could have been used while still achieving the same spectral resolution at the same exposure level. Note that the calculations presented in this section refer to a narrow-band source, while higher optical power levels would be needed if a broad-band light source were utilized, spanning larger number of columns on the camera.

Overall, through utilizing a significantly lower light level, we can satisfy the light budget needs of the scenario presented in Fig. 5, whose power levels are depicted in Fig. 6 (necessitating 38 nW of light power at the camera, at 200 kHz A-Scan rate) Further improvement could be achieved with electronic gain applied on the acquired images (0 dB gain was used throughout the experiments), whose investigation is left as a future work.

Fig. 6 also plots the power budget calculations for non-guiding scatterer (scatterer # 10) showcasing the same spectral resolution as the waveguide scatterer (scatterer #25). Moreover a third plot is added showing the ideal power budget for a 2D scattering waveguide (with possibly dielectric stack walls for perfect reflection) that does not let any light out within its length.

Without loss of generality, the calculations presented here could be revised for other conditions (other tissues, sensor arrays etc.).

VII. Conclusions and Discussion

Using a scatterer that is sandwiched between two metal dies, we demonstrated an optical-efficiency enhanced speckle-enhanced prism spectrometer. Among a plethora of scatterers (both non-guiding, and waveguide type) under test, we were able to i) demonstrate up to an order of magnitude better spectral resolution for a given optical efficiency with the waveguide scatterer, as opposed to conventional scatterer, and ii) up to two orders of magnitude better optical efficiency for a given spectral resolution. Such an improvement in optical efficiency is specifically critical in applications, which require rapid data acquisition ($\sim$100 kHz A-scan rates) with low light power, such as Ophthalmologic applications of Optical Coherence Tomography. The light budget calculations show that the spectrometer presented here can handle such speeds, given that a linear sensor array supporting the desired A-scan rate is used, as opposed to a conventional CCD camera.

As a future work, we plan on demonstrating a 2D scattering waveguide manufactured using four highly reflective walls (exploiting dielectric mirrors) to potentially gain another 2-order of magnitude improvement in optical efficiency.

References

[1] B. Redding, M. Alam, M. Seifert, and H. Cao, "High-resolution and broadband all-fiber spectrometers," *Optica*, vol. 1, no. 3, pp. 175–180, 2014.
[2] N. H. Wan, F. Meng, T. Schröder, R.-J. Shiue, E. H. Chen, and D. Englund, "High-resolution optical spectroscopy using multimode interference in a compact tapered fibre," *Nature Commun.*, vol. 6, 2015, Art. no. 7762.
[3] S. Kaan Çetindağ, M. F. Toy, O. Ferhanoglu, and F. Civitci, "A speckle-enhanced prism spectrometer with high dynamic range," *IEEE Photon. Technol. Lett.*, vol. 30, no. 24, pp. 2139–2142, Dec. 2018.
[4] B. Redding, S. M. Popoff, and H. Cao, "All-fiber spectrometer based on speckle pattern reconstruction," *Opt. Exp.*, vol. 21, no. 5, pp. 6584–6600, 2013.
[5] G. Häusler and M. W. Lindner, "'Coherence Radar' and 'Spectral Radar'—New tools for dermatological diagnosis," *J. Biomed. Opt.*, vol. 3, no. 1, pp. 21–31, 1998.
[6] D. K. Sardar, G. Y. Swanland, R. M. Yow, R. J. Thomas, and A. T. C. Tsin, "Optical properties of ocular tissues in the near infrared region," *Lasers Med. Sci.*, vol. 22, no. 1, pp. 46–52, 2007.
[7] A. M. Bagci, M. Shahidi, R. Ansari, M. Blair, N. P. Blair, and R. Zelkha, "Thickness profiles of retinal layers by optical coherence tomography image segmentation," *Amer. J. Ophthalmol.*, vol. 146, no. 5, pp. 679–687, 2008.
[8] S. Gigan, "Optical microscopy aims deep," *Nature Photon.*, vol. 11, no. 1, pp. 14–16, 2017.
[9] IEC, *Safety of Laser Products*, Geneva, Switzerland, 2014.
[10] B. G. Yust, L. C. Mimun, and D. K. Sardar, "Optical absorption and scattering of bovine cornea, lens, and retina in the near-infrared region," *Lasers Med. Sci.*, vol. 27, no. 2, pp. 413–422, 2012.
[11] D. F. Swinehart, "The Beer-Lambert law," *J. Chem. Educ.*, vol. 39, no. 7, pp. 333–335, 1962.

Sakir Kaan Çetindağ was born in Izmir, Turkey in 1993. He received the B.Sc. degree in electrics and electronics engineering from Koç University, Istanbul, Turkey, in 2015 and the M.Sc. degree in biomedical engineering from Istanbul Technical University, Istanbul. He is currently working toward the Ph.D. degree with the Neuro-Electronics Research Flanders, IMEC, Leuven, Belgium. His research interests include biomedical optics, bioinformatics, and neuroengineering.

Muhammed Fatih Toy received the bachelor's and master's degrees in electrical and electronics engineering from Koç University, Istanbul, Turkey, in 2006 and 2008, respectively. He received the Ph.D. degree in photonics from École Polytechnique Fédérale de Lausanne, Lausanne, Switzerland, in 2013. He is an Assistant Professor of Biomedical Engineering with Istanbul Medipol University, Istanbul. Subsequently, he took part in the establishment of a start-up company named Nanolive SA where he serves as a Technical Advisor. His research interests include coherent imaging, digital holography, superresolution microscopy, and near to eye displays.

Onur Ferhanoğlu received the B.S. and M.S. degrees in electrical engineering from Bilkent University, Ankara, Turkey, in 2003 and 2005, respectively. He joined Koç University as a Graduate Researcher to develop MEMS thermal imaging sensors, in 2005. From 2011 to 2014, he was a Postdoctoral Fellow with the University of Texas at Austin, TX, USA, where he played a key role in the development of an ultrafast laser microsurgery scalpel. He is currently appointed with the Electronics and Communication Engineering Department, Istanbul Technical University, Istanbul, Turkey. His research interests are biomedical optic and MEMS.

Fehmi Çivitci received the B.S. and M.S. degrees from Middle East Technical University, Ankara, Turkey, in 2005 and 2008, respectively. He received the Ph.D. degree from the University of Twente, Enschede, Netherlands, in 2014. From 2013 to 2015, he worked as a Researcher with the Optical Micro-Systems Laboratory, Koç University. In 2015, he joined the Department of Electronics and Communication Engineering, Istanbul Technical University, Istanbul, Turkey, as a Faculty Member. He is currently working as an Associate Scientist with the Oregon Health and Science University, Portland, OR, USA, focusing on early cancer detection.